Spatio-temporal Characteristics of Frictional Properties on the Subducting Pacific Plate Off the East of Tohoku District, Japan Estimated from Stress Drops of Small Earthquakes

Takuji Yamada (takuji.yamada.t9sci@vc.ibaraki.ac.jp)
Ibaraki University https://orcid.org/0000-0001-6630-3686
Meitong Duan
Ibaraki University (Graduated)
Jun Kawahara
Ibaraki University

Full paper

Keywords: Frictional properties, Pacic Plate, Stress drop, Spatio-temporal pattern, Small earthquake, East coast of the Tohoku district, 2011 Tohoku earthquake

Posted Date: July 2nd, 2020

DOI: https://doi.org/10.21203/rs.3.rs-39395/v1

Version of Record: A version of this preprint was published on January 18th, 2021. See the published version at https://doi.org/10.1186/s40623-020-01326-8.

Spatio-temporal characteristics of frictional properties on the subducting Pacific Plate off the east of Tohoku district, Japan estimated from stress drops of small earthquakes

Takuji Yamada[1], Faculty of Science, Graduate School of Science and Engineering, Ibaraki University, Ibaraki 310-8512, Japan, takuji.yamada.t9sci@vc.ibaraki.ac.jp

Meitong Duan[2], Department of Science, Graduate School of Science and Engineering, Ibaraki University, Ibaraki 310-8512, Japan, meitong.suihan@gmail.com

Jun Kawahara[1], Faculty of Science, Graduate School of Science and Engineering, Ibaraki University, Ibaraki 310-8512, Japan, jun.kawahara.ri@vc.ibaraki.ac.jp

Preprint submitted to *Earth, Planets and Space* on June 30, 2020

Abstract

The east coast of the Tohoku district, Japan has a high seismicity, including aftershocks of the 2011 M9 Tohoku earthquake. We analyzed 1142 earthquakes with $4.4 \leq M_W \leq 5.0$ that occurred in 2003 through 2018 and obtained spatio-temporal pattern of stress drop on the Pacific Plate that subducts beneath the Okhotsk Plate. Here we show that small earthquakes at edges of a region with a large slip during the 2011 Tohoku earthquake had high values of stress drop, indicating that the areas had a high frictional strength and suppressed the coseismic slip of the 2011 Tohoku earthquake. In addition, stress drops of small earthquakes in some of the areas likely decreased after the 2011 Tohoku earthquake. This indicates that the frictional strength decreased at the areas due to the following aftershocks of the 2011 Tohoku earthquake, consistent with a high aftershock activity. This also supports that the frictional properties on a subducting plate interface can be monitored by stress drops of small earthquakes, as pointed out by some previous studies.

Keywords

Frictional properties, Pacific Plate, Stress drop, Spatio-temporal pattern, Small earthquake, East coast of the Tohoku district, 2011 Tohoku earthquake

Background

Tectonics and characteristics of earthquakes off the east coast of the Tohoku district, Japan

Numerous large earthquakes as well as the huge 2011 Tohoku earthquake with M_W 9.0 have been observed off the east coast of the Tohoku district, Japan, associated with the subduction of the Pacific Plate beneath the Okhotsk Plate at a rate of 80-100 mm/year DeMets et al. (1990). Some previous studies have suggested the spatial heterogeneity of the frictional properties on the plate interface in this region. Yamanaka and Kikuchi (2004) analyzed source processes of large interplate earthquakes that occurred off the east coast of the Tohoku district, Japan and found that areas with a large coseismic displacement, where they refer to as asperities, distributed as stepping stones. They also pointed out that the typical size of individual asperities in northeastern Japan was M7 class and that an M8 class earthquake could be caused when several asperities were synchronized. Nishikawa et al. (2019) analyzed waveforms of

slow earthquakes observed by the new S-net ocean-bottom seismic network and investigated their spatial distribution along the Japan Trench. They found that the area that ruptured during the 2011 Tohoku earthquake was bounded by areas that have large numbers of slow earthquakes. They reported that a segmentation likely caused to cease the coseismic rupture of the 2011 Tohoku earthquake, which provides important information for a risk assessment from future major earthquakes. Baba et al. (2020) detected very low frequency earthquakes (VLFEs) off the Hokkaido and Tohoku Pacific coasts by a matched-filter technique. They pointed out that their spatial distribution is consistent with the afterslip of the 2003 Tokachi-Oki earthquake (M_W 8.0). They also found that the VLFE activity inside a large coseismic slip area of the 2011 Tohoku earthquake was low thereafter, whereas outside the area, VLFE activity increased after the 2011 Tohoku earthquake. These results suggest that there is significant spatial heterogeneity of the frictional properties on the plate interface in this region.

As many small earthquakes have been occuring on the subducting Pacific Plate off the east coast of the Tohoku district, they provide a good opportunity for investigating the pattern of their stress drops in both space and time and its implication with respect to the frictional properties on the plate interface. In this study, we investigated stress drops of these small earthquakes following the method of Yamada et al. (2010, 2015, 2017) and discussed the correlation of their spatial pattern with slip distribution of the 2011 Tohoku earthquake and other large historical earthquakes. In the next subsection, we summarize the significance of stress drop analysis.

Significance of analysis on stress drop

Stress drop is an important source parameter which indicates the difference between the initial and residual stress levels associated with an earthquake, that is, the shear stresses before and after the earthquake rupture. Stress drop of small and large earthquakes have been investigated and have almost confirmed the self-similarity of earthquakes (Kanamori and Anderson (1975); Abercrombie (1995); Prieto et al. (2004); Yamada et al. (2005, 2007); Kwiatek et al. (2011); Yoshimitsu et al. (2014)). This self-similarity is important in that we can use values of stress drop as indicators of the difference between the shear strength and the dynamic stress level on the fault plane, independent of the earthquake size. We have to note here that the self-similarity of earthquakes for a broad range of magnitude remains a matter of debate and is not fully confirmed. Some studies have pointed out that earthquakes might have a weak dissimilarity Malagnini et al. (2008). However, small earthquakes with a narrow magnitude range, as considered in this study, do not indicate a strong dissimilarity and their stress drops can be treated

as an indicator of frictional properties.

Heterogeneity of stress and strength in space and time has been investigated by stress drops of earthquakes, especially for the last fifteen years. Allman and Shearer (2007) estimated stress drops of small earthquakes near Parkfield, California and investigated relationships of their spatial and temporal variations around the source region of the 2004 Parkfield earthquake. They concluded that earthquakes around the coseismic rupture area of the 2004 Parkfield earthquake had higher values of stress drop compared to the values of earthquakes outside the region. For even finer scale, Yamada et al. (2010) investigated stress drops of small earthquakes which occurred on the fault plane of the 2006 Kīholo Bay earthquake with M_W 6.7 and discussed the spatial characteristics of stress drop compared to the coseismic slip distribution of the earthquake. They found that small earthquakes around patches with a large displacement during the main shock had larger values of stress drop and concluded that the spatial pattern of the stress drop reflects coherent variations in the difference of strength and the residual stress level. Urano et al. (2015) carried out a similar analysis for the 2007 Noto Hanto earthquake and pointed out that static stress drops of aftershocks in the area with a large coseismic slip during the mainshock are larger than those in a small slip area. This result also suggests that *in-situ* frictional properties can be estimated from stress drops of small earthquakes, the same as the conclusion of Yamada et al. (2010). Oth (2013) calculated stress drops of earthquakes in Japan and concluded that the values had strong correlation with heat flow variations. Yamada et al. (2015) investigated a cluster earthquake activity in the Tanzawa Mountains region, Japan and found that the activity showed the hypocenter migration and consisted of earthquakes with a small stress drop. They concluded that the activity would be triggered by the increase of pore pressure due to fluid, that is, the decrease of the shear strength. Yamada et al. (2017) analyzed stress drops of small earthquakes off the Pacific coast of Hokkaido, Japan and found that the spatial pattern in stress drops has a good correlation with spatial characteristics of coseismic displacements during individual historical large earthquakes. Moyer et al. (2018) estimated stress drops of small earthquakes ($2.3 \leq M_W \leq 4.0$) on Gofar transform fault at the East Pacific Rise and found an inverse correlation between stress drop and the reduction of P wave velocity, which they interpreted as the effect of damage around the fault zone. They also pointed out that earthquakes following the mainshock ($M_W 6.0$) had lower values of stress drop, consistent with increased damage and decreased fault strength after a large earthquake. Although estimation of stress drop in general includes some assumptions such as circular faults explained in the next section, these previous studies strongly suggest that the results of stress drop indicate actual physical

characteristics on fault planes of earthquakes.

Some studies, on the other hand, raised questions if the values of estimated stress drop reflect frictional properties. Shearer et al. (2006) analyzed stress drops of aftershocks associated with the 1992 Landers earthquake and investigated the relationship of their spatial pattern to the coseismic slip on three major segments derived by Wald and Heaton (1994). They found that stress drops of aftershocks on the northern segment (Camp Rock/Emerson faults) had a good correlation with the slip distribution. However, they also pointed out that the values on the southern segment (Landers/Johnson Valley faults) showed a weaker consistency and they were anti-correlated on the central segment (Homestead Valley fault). Hardebeck and Aron (2009) investigated stress drops of earthquakes on Hayward fault. They found that stress drops were well correlated with an applied shear stress but did not show a direct correlation with the proposed strength of the wall-rock geology. As they noted, this suggests that the stress drop would give an information on the fault strength, but the relation between fault strength and the strength of wall rock would be complex. Our result will provide an example whether or not stress drops estimated from seismograms can be used for investigating frictional properties on earthquake faults.

Methods

Following the method of Yamada et al. (2010, 2015, 2017), we investigated stress drops of 1142 small earthquakes ($4.4 \leq M \leq 5.0$) off the east coast of Tohoku district, Japan, that occurred in 2003 through 2018 (Fig.1). Both of the earthquakes before and after the 2011 M9 Tohoku earthquake are included in the analysis. Note that M indicates the magnitude of an earthquake as determined by the Japan Meteorological Agency (JMA) in this paper. The hypocenters of the 1142 earthquakes were located 35.0° N through 41.5° N and 140.5° E through 145.0° E in latitude and longitude directions, respectively, with a depth of ±15 km from the interface of the Pacific Plate, which had been derived by Nakajima and Hasegawa (2006). Because of the poor azimuthal coverage of seismic stations, the distance of 15 km in depth direction is within the range of uncertainty in the hypocenter estimation in the study area. We analyzed waveforms recorded at stations, which have been maintained by National Research Institute for Earth Science and Disaster Resillience, Japan (NIED), Hokkaido University, Hirosaki University, Tohoku University, and JMA.

An observed waveform as a function of time $W(t)$ includes the effects of the source $S(t)$, the path from a hypocenter to a seismic station $P(t)$, site amplification effects $A(t)$, and the instrumental responce of

a seismometer $I(t)$, that is:

$$W(t) = S(t) * P(t) * A(t) * I(t), \tag{1}$$

where the operator $*$ indicates convolution. Because the convolution is expressed as a scalar product in the frequency domain, the following equation holds:

$$W(f) = S(f) \cdot P(f) \cdot A(f) \cdot I(f), \tag{2}$$

where $W(f)$, $S(f)$, $P(f)$, $A(f)$, and $I(f)$ are expressions of $W(t)$, $S(t)$, $P(t)$, $A(t)$, and $I(t)$ in the frequency domain, respectively. If we know the functions of $P(f)$, $A(f)$, and $I(f)$, we can then obtain the Green's function and extract the source effect from the observed waveform. As it is difficult in actual to estimate the Green's function precisely, we adopted the method of empirical Green's function (EGF) (Hartzell (1978)).

The observed seismograms of two earthquakes at a receiver can be expressed as follows:

$$W_1(f) = S_1(f) \cdot P_1(f) \cdot A_1(f) \cdot I(f), \tag{3}$$

$$W_2(f) = S_2(f) \cdot P_2(f) \cdot A_2(f) \cdot I(f). \tag{4}$$

If the hypocenters of the two earthquakes are identical, the soil beneath the seismic station acts linearly independent of the amplitude of the incoming waveforms, and no velocity change takes place during the two earthquakes, then the path and site effects are exactly the same, which shows

$$P_1(f) = P_2(f), \tag{5}$$

and

$$A_1(f) = A_2(f). \tag{6}$$

In this case, we can derive the ratio of source effects on two earthquakes by calculating the ratio of the observed waveforms in the frequency domain,

$$\frac{W_1(f)}{W_2(f)} = \frac{S_1(f) \cdot P_1(f) \cdot A_1(f) \cdot I(f)}{S_2(f) \cdot P_2(f) \cdot A_2(f) \cdot I(f)} = \frac{S_1(f)}{S_2(f)}. \tag{7}$$

Eq. (7) gives the spectral ratio of each pair of an analyzed and an EGF earthquakes. It is assumed in this study that source spectrum of an earthquake $S^C(f)$ can be expressed by the omega-squared model of Boatwright (1978), which is formulated as follows:

$$S^C(f) = R^C(f) \cdot M_0^C(f) \cdot \left\{ \frac{1}{1 + \left(f/f_0^C\right)^4} \right\}^{1/2}, \tag{8}$$

where R, M_0, and f_0 are the coefficient of the radiation pattern, the seismic moment, and the corner frequency of the earthquake, respectively. C indicates the wave type, which corresponds to either P or S. This assumption suggests that we approximated the fault as a circular plane. The deconvolved spectra of velocity $|\dot{u}_r^C(f)|$ can then be expressed by the following equation:

$$\begin{aligned}\left|\dot{u}_r^C(f)\right| &= \left|\frac{S_A^C(f)}{S_E^C(f)}\right| = \frac{R_A^C \cdot M_{0A}}{R_E^C \cdot M_{0E}} \cdot \left\{\frac{1+\left(f/f_{0E}^C\right)^4}{1+\left(f/f_{0A}^C\right)^4}\right\}^{1/2} \\ &= R_r^C M_{0r} \cdot \left\{\frac{1+\left(f/f_{0E}^C\right)^4}{1+\left(f/f_{0A}^C\right)^4}\right\}^{1/2}, \end{aligned} \tag{9}$$

where subscripts A and E correspond to analyzed and EGF earthquakes, respectively. Moreover, R_r^C and M_{0r} indicate the relative values of R_A^C/R_E^C and M_{0A}/M_{0E}, respectively. The value of R_r^C is equal to 1 if the focal mechanisms and hypocenters of the analyzed and EGF earthquakes are exactly the same. The sampling rate of waveforms analyzed in this study was 100 Hz. We used waveforms of earthquakes in 2012 through 2018 (after the 2011 Tohoku earthquake) with M3.5 which were closest to the hypocenters of the analyzed earthquakes as the EGFs. A list of analyzed and EGF earthquakes in this study is available as an additional file (refer to eqlist.txt).

We adopted earthquakes with M3.5 as EGFs and analyzed corner frequencies of earthquakes in a relatively narrow magnitude range ($4.4 \leq M \leq 5.0$). This treatment is based on the following considerations. In order to ensure a good signal-to-noise ratio of EGFs, especially for spectra of lower frequencies, we used waveforms of earthquakes with M3.5 as EGFs. The lower limit (M4.4) of the analyzed earthquakes was set for keeping a difference in magnitude of about 1 compared to the EGFs and ensuring quality in estimating the corner frequencies. As stress drops are calculated for individual earthquakes, the values for large earthquakes would represent the average characteristics of individual large fault planes. This is not good condition because the values of stress drop for large earthquakes might not reflect local frictional characteristics. We can avoid this problem by adopting an upper limit of magnitude for analyzing stress drops of earthquakes. In addition, as waveforms of some large earthquakes were clipped, we fixed the maximum size of earthquake to M5.0 in the analysis.

We estimated the spectral ratios of P and S waves for individual pairs of an earthquake and an EGF. The spectral ratios were analyzed for three time windows with a length of 1024 data points, or 10.23 s. The begining of the first time window were set to be 0.50 s prior to the arrival times of either the P or S waves. The elapsed times of the two successive time windows were set to be 1.28 and 2.56 s, respectively.

The spectral ratio can be approximated as following equations by taking the logarithm of Eq. (9):

$$\ln\left|\dot{u}_r^C(f)\right| \approx g\left(f; f_{0A}^C; f_{0E}^C\right), \tag{10}$$

$$g\left(f; f_{0A}^C; f_{0E}^C\right) = \ln\left(R_r^C M_{0r}\right) - \frac{1}{2}\ln\left\{1+\left(f/f_{0A}^C\right)^4\right\} + \frac{1}{2}\ln\left\{1+\left(f/f_{0E}^C\right)^4\right\}. \tag{11}$$

Before fitting individual analyzed spectral ratios with the theoretical function expressed by Eqs. (10) and (11), we resampled the data points so that the interval in frequency was equal to 0.05 on a $\log_{10}$ scale. As a result, we obtained 20 data points (frequency bands) for each order of frequency. This procedure allowed us to treat high- and low-frequency data equivalently. We also estimated the standard deviation of the spectral ratio for each frequency band and used the value as a weight in fitting data, as explained below.

We investigated the values of $R_r^C M_{0r}$, f_{0A}^C, and f_{0E}^C in Eq. (11) for each station by a grid search that gave the minimum residual for the spectral ratios of three time windows, similar to Imanishi and Ellsworth (2006). Here values of residual R can be defined by the following equation,

$$R = \Sigma_i \frac{\left\{\ln \dot{u}_r^C(f) - g\left(f; f_{0A}^C; f_{0E}^C\right)\right\}^2}{\sigma_i^2} \tag{12}$$

where σ_i is the standard deviation for each frequency band calculated in resampling the spectral ratio. All of the earthquakes analyzed in this study have four or more stations available for the corner frequency estimation. We used data within the frequency range of 0.7 Hz through 20 Hz to calculate the residual in Eq. (12) and investigated corner frequencies by grid search between 0.3 and 20 Hz. This frequency range and the length of the time window (10.23 s, or 1024 data points) were adopted so that corner frequencies of earthquakes with $4.4 \leq M \leq 5.0$ could be estimated correctly, which would be around 1-3 Hz as expected by the self-similarity of earthquakes. Fig. 2 shows an example of the corner frequency analysis, including S-wave velocity seismograms, their spectra, deconvolved spectra after the resampling, and the obtained curves of spectral ratio that were used for investigating a corner frequency. Another example is provided as a supplemental figure Fig. A1, which shows the analysis for the P wave for the same earthquake and the same station as shown in Fig. 2. Examples for another earthquake are also provided as supplemental figures (Figs. A2 and A3). We confirm that waveforms have a good signal-to-noise ratio larger than a factor of five even for low frequencies between 0.7 and 2 Hz for EGF earthquakes.

Finally, we estimated the values of stress drop following Madariaga (1976):

$$\Delta\sigma^C = \frac{7}{16} M_{0A} \left(\frac{f_{0A}^C}{kV_S} \right)^3, \tag{13}$$

where V_S is the shear wave velocity, which we set 4.5 km/s refering to Matsubara and Obara (2011), and C corresponds to the wave type (P or S). The seismic moment M_0 in newton meters (Nm) can be calculated from M_W using the following equation Hanks and Kanamori (1979): $\log_{10} M_0 = 1.5M_W + 9.1$. We fixed the value k as 0.32 and 0.21 for P and S waves, respectively, assuming that the rupture of earthquakes expanded with a speed of $0.9V_S$ Madariaga (1976). We will discuss the effect of the value k in the section "Discussion." It is assumed in this study that M is equivalent to the moment magnitude M_W in calculating stress drops. The validity of this assumption will also be discussed in the section "Discussion."

Results

Spatial pattern of stress drop

Figs. 3 and 4 show the spatial distribution of stress drop estimated from P and S waves, which are superposed on the coseismic slip distribution of large earthquakes, including the 2011 Tohoku earthquake. The results of individual earthquakes in Figs. 3(a)(c) are available as Additional files (refer to results_P.txt and results_S.txt). Both of the results derived from P and S waves indicate spatial heterogeneity on stress drop, suggesting that the frictional properties on the Pacific plate are heterogeneous in space.

We found that areas with a large coseismic displacement during the 1968 Tokachi-oki earthquake have higher values of stress drop. This is consistent with the result of Yamada et al. (2017) and suggests that these areas have higher shear strength. Similarly, an area with a large stress drop can be seen at the south-east tip of the coseismic displacement during the 1978 Miyagi-oki earthquake. It is likely that the area acted as a barrier because of a higher shear strength in 1978, whereas it had been included inside the source area in 1936. In addition, the areas marked as A and B in Fig. 4 have a higher value of stress drop. Both of the areas coincide with the regions where moderate-sized earthquakes regularly take place every several years (Uchida et al. (2007); Okuda and Ide (2018)). These results can also be reasonably explained that there is significant spatial heterogeneity in frictional properties and these areas have a higher shear strength.

However, we have to note that slip distributions obtained by the waveform inversion may include large

uncertainty (Mai et al. (2016)). The significance of the results, as well as the discrepancy between the absolute values of stress drop derived from P and S waves will be discussed in the section "Discussion."

Temporal change of stress drop: Effects of the 2011 Tohoku earthquake

We would also like to point out the temporal change in stress drop associated with the 2011 Tohoku earthquake. Fig. 5 shows spatial patterns of stress drop before and after the 2011 Tohoku earthquake, as well as that estimated from all the earthquakes analyzed in this study (2003 through 2018). Areas marked as C and D, which correspond to western tips of the large coseismic displacement during the 2011 Tohoku earthquake, have higher values of stress drop before the earthquake (Fig. 5a). After the 2011 Tohoku earthquakes, values of stress drop in these areas decreased to the value around the average all over the study area as shown in Fig. 5(b). Fig. 6 shows stress drops of analyzed earthquakes as a function of depth and seismic moment, as well as the temporal changes. Stress drops of earthquakes show no clear dependency on depth, seismic moment, and time. Therefore, the temporal changes in Figs. 5(a)(b) and 6(d)(e) suggest the changes of frictional properties in time and are not artifacts nor apparent ones.

We discuss these results from physical point of view in the next section.

Discussion

Interpretation of our results from the physical viewpoint of earthquake rupture

We found that earthquakes at edges of a large coseismic slip with a large gradient in displacement during the 2011 Tohoku earthquake show a high value of stress drop. As mentioned in the subsection 1.2, stress drop is an indicator of the difference between the shear strength and the dynamic stress level. Therefore, the spatial pattern obtained in this study likely to reflect the spatial heterogeneity in frictional properties on the plate interface between the Pacific and Okhotsk plates.

In addition, stress drops of earthquakes at the above area seem to decrease after the 2011 Tohoku earthquake. This would indicate a gradual weakening of the shear strength due to the stress concentration associated with the coseismic slip during the 2011 Tohoku earthquake (Ohnaka and Shen (1999)). Another possibility would be an effect of fluid (Yamada et al. (2015)). As fluid confined in a crack on the plate interface can reduce the normal stress, the increase of fluid pressure can decrease the shear strength, resulting in a smaller stress drop.

It is true that a smaller stress drop would be observed if the dynamic stress level increased for some reason. However, it would be hard to be the case. Di Toro et al. (2011) pointed out that the dynamic

stress level depends on the slip velocity; a slower slip velocity gives a higher dynamic stress level. If the decrease of stress drop were caused by a slow-down of the slip velocity, all the events after the 2011 Tohoku earthquake had to have a slower slip velocity. If this were the case, observed waveforms would have shown some notable change of their characteristics, which we did not observe at all. Therefore, we conclude that the observed temporal change in stress drop would be caused not by the increase of the dynamic stress level, but the decrease of the shear strength due to the stress concentration associated with the coseismic slip of the 2011 Tohoku earthquake.

Comparison to previous studies

Uchide et al. (2014) investigated spatial pattern of stress drop before the 2011 Tohoku earthquake in the same region by a method different from that of this paper. The spatial distribution of stress drop before the 2011 Tohoku earthquake in our results is very much consistent with that shown in Uchide et al. (2014), suggesting the robustness of our analysis. However, there is a discrepancy between the two results. Although Uchide et al. (2014) insisted that they found a strong increase in stress drop with depth between 30 km and 60 km, such an increase cannot be seen in our result (Fig. 6). We are not sure of the reason, but one possibility would be the difference of waveforms used as empirical Green's functions. We used waveforms of earthquakes (M3.5) in the vicinity of individual analyzed earthquakes with a good signal-to-noise ratio for all over the frequency band used in the analysis (Figs. 2, A1, A2 and A3) as local empirical Green's functions so that fine-scale heterogeneity can be detected. Accumulation of the *in-situ* seismic data, including ones observed by S-net (Kubota et al. (2020)), would provide good opportunity for investigating source characteristics, such as stress drop, of earthquakes with higher precision in the region analyzed in this paper in the near future.

Difference of stress drops from P and S waves

As each earthquake has one value of stress drop, the value of stress drop for an earthquake calculated from P wave should be the same as the value derived from S wave. However, our results in Figs. 3 and 4 indicate that the absolute values of stress drop deduced from P waves are much lower than the values derived from S waves. This discrepancy originates from the value of k in Eq. (13), that is, the assumed rupture speed in the model. Hence, the discrepancy provides an insight into the rupture characteristics of analyzed small earthquakes, as described in detail in Yamada et al. (2017). We briefly explain the significance of the discrepancy here.

The model of Madariaga (1976), which is used in this study and is commonly adopted in stress drop

estimation, assumes that the rupture initiates from the center of a circular fault plane and propagates with a certain rupture speed that is slower than the P-wave velocity. The values of 0.32 and 0.21 for constant k in Eq. 13 depend on the assumed rupture speed, which we fixed to be 90% of the S-wave velocity V_S. These factors become smaller for a slower rupture propagation, and the value k for P wave is much more sensitive to the rupture speed than that for S wave (Madariaga (1976)). As the estimated values of stress drop from P waves in our study are smaller than those from S waves, slower rupture speeds result in the values of stress drop being closer. Thus, our results suggest that the actual rupture speed of the analyzed earthquakes would be slower than $0.9V_S$. This is consistent with many studies of source process that reported the rupture on a fault plane propagates with a speed of $70 - 80\%$ of V_S, independent of earthquake magnitude (Wald and Heaton (1994); Yamada et al. (2005)), with a few exceptions (Ji et al. (2002); Walker and Shearer (2009)).

Stress drops derived from P and S waves in Figs. 3 and 4 show exactly the same spatial pattern. This strongly suggests that our results for stress drop are stably estimated and that their lateral characteristics indicates the spatial heterogeneity of the frictional properties on the interface of the subdcting Pacific Plate in the study area.

Validity associated with the assumption of $M = M_W$

We estimated stress drops under the assumption that the value of M determined by JMA is equivalent to M_W. As our results might include an artifact due to this assumption, we investigated its validity. Fig. 7 shows the relationship between M and values of $3.5 + (2/3)\log_{10}\left(R_r^C M_{0r}\right)$ in Eq. (9) for individual earthquakes, which correspond to moment magnitudes of analyzed earthquakes if individual pairs of analyzed and EGF earthquakes have identical focal mechanisms ($R_r^C = 1$) and if the values of M_W for EGF earthquakes are 3.5 (M3.5 = M_W3.5). We herein refer to the value of $3.5 + (2/3)\log_{10}\left(R_r^C M_{0r}\right)$ as apparent magnitude. As we adopted earthquakes with M3.5 as EGFs, Fig. 7 suggests that the actual values of M_W would be slightly smaller than M values, which is consistent with Uchide and Imanishi (2018). This result implies that the absolute values of stress drop derived in this study might be overestimated. However, Fig. 7 shows a clear linear relationship between the two parameters with a slope of 1. This fact strongly suggests that the spatial pattern in stress drop obtained in this study is reliable.

Conclusion

We summarize our conclusion as follows.

(1) Areas with a high stress drop are located at edges of a large coseismic slip with a high gradient in displacement during the 2011 Tohoku earthquake.

(2) The areas with a high stress drop showed temporal change on values of stress drop after the 2011 Tohoku earthquake.

(3) The fact (2) may indicate a gradual weakening of the shear strength due to the stress concentration associated with the coseismic slip during the 2011 Tohoku earthquake Ohnaka and Shen (1999).

(4) Temporal change in stress drop likely to reflect the change in the shear strength. As the dynamic stress level depends on the slip velocity Di Toro et al. (2011), our results can hardly be explained as the change in the dynamic stress level.

Our results suggest that the frictional properties on a subducting plate interface can be monitored by stress drops of small earthquakes, as pointed out by some previous studies including Yamada et al. (2017), which provides important information for strong motion estimation due to future large earthquakes.

List of abbreviations

JMA: Japan Meteorological Agency

M_W: Moment magnitude

NIED: National Research Institute for Earth Science and Disaster Resilience, Japan

Availability of data and materials

Waveform data that are analyzed in this study can be downloaded from the website of Hi-net, NIED (https://www.hinet.bosai.go.jp). A list of earthquakes analyzed in this study and their stress drops estimated from P and S waves are available as following supplementary information files; eqlist.txt, result_P.txt, and result_S.txt, respectively.

Competing interests

The authors declare that they have no competing interests.

Funding

Not applicable.

Authors' contributions

TY designed the research project, conducted the analysis, and wrote the manuscript. MD carried out preliminary analyses. JK participated in the discussion of the results. All of the authors read and approved the final manuscript.

Authors' information

1. Department of Earth Sciences, Faculty of Science, Ibaraki University, 2-1-1 Bunkyo, Mito, Ibaraki 310-8512, Japan. 2. Department of Science, Graduate School of Science and Engineering, Ibaraki University, 2-1-1 Bunkyo, Mito, Ibaraki 310-8512, Japan.

Acknowledgments

The authors would like to express our sincere thanks to the two reviewers (AAA AAA and BBB BBB), and the editor CCC CCC, for their insightful comments and suggestions, which helped us improve our manuscript. We used waveforms that had been observed at stations of Hi-net (NIED), as well as Hokkaido Univ., Hirosaki Univ., Tohoku Univ. and JMA, which can be downloaded from the NIED Hi-net website (https://www.hinet.bosai.go.jp). The authors would like to thank the individuals who have been maintaining these seismic stations. We also used arrival times of P and S waves which were determined by JMA. The authors would also like to express our gratitudes to Takeshi Iinuma and Yoshiko Yamanaka for providing the results of coseismic displacements. Figures were created using Generic Mapping Tools software Wessel and Smith (1995).

Appendix A. Other examples of the corner frequency analyses

In addition to Fig. 2, we will show three examples of deconvolved spectra as well as waveforms in time and frequency domains (Figs. A1, A2, and A3). We can see waveforms analyzed have good signal-to-noise ratios and confirm that deconvolved spectra are well fitted by the omega-squared model.

References

Abercrombie RE (1995) Earthquake source scaling relationships from -1 to 5 M_L using seismograms recorded at 2.5-km depth. J Geophys Res 100, B12:24015-24036

Allman BP, Shearer PM (2007) Spatial and temporal stress drop variations in small earthquakes near Parkfield, California. J Geophys Res 112:B04305, doi:10.1029/2006JB004395

Baba S, Takeo A, Obara K, Matsuzawa T, Maeda T (2020) Comprehensive detection of very low frequency earthquakes off the Hokkaido and Tohoku Pacific coasts, northeastern Japan. J Geophys Res 125: e2019JB017988

Boatwright J (1978) Detailed spectral analysis of two small New York State earthquakes. Bull Seismol Soc Am 68:1117-1131

Demets C, Gordon RG, Argus DF, Stein S (1990) Current plate motions. Geophys J Int 101:425-478

Di Toro G, Han R, Hirose T, De Paola N, Nielsen S, Mizoguchi K, and Ferri F, Cocco M, Shimamoto T (2011) Fault lubrication during earthquakes. Nature 471:494, doi:10.1038/nature09838

Hanks, T, Kanamori H (1979) A moment magnitude scale. J Geophys Res 84:2348-2350

Hardebeck JL, Aron A (2009) Earthquake stress drops and inferred fault strength on the Hayward fault, east San Francisco Bay, California. Bull Seismol Soc America 99:1801-1814

Hartzell SH (1978) Earthquake aftershocks as Green's functions. Geophys Res Lett 5:1-4

Iinuma T, Hino R, Kido M, Inazu D, Osada Y, Ito Y, Hozono M, Tsushima H, Suzuki S, Fujimoto H, Miura S (2012) Coseismic slip distribution of the 2011 off the Pacific Coast of Tohoku Earthquake (M9.0) refined by means of seafloor geodetic data. J Geophys Res 117, B7, doi:10.1029/2012JB009186

Imanishi K, Ellsworth WL (2006) Source scaling relationships of microearthquakes at Parkfield, CA, determined using the SAFOD pilot hole seismic array. In: Abercrombie RE, McGarr A, Kanamori H, Di Toro G (eds) Earthquakes: radiated energy and the physics of earthquake faulting, vol 170, Geophys Monogr Ser. AGU, Washington D.C, pp 81–90

Ji C, Wald DJ, Helmberger DV (2002) Source description of the 1999 Hector Mine, California, earthquake, part I: Wavelet domain inversion theory and resolution analysis. Bull Seismol Soc Am 92:1192-1207

Kanamori H, Anderson DL (1975) Theoretical basis of some empirical relations in seismology. Bull Seismol Soc Am 65:1073-1095

Kita S, Okada T, Hasegawa A, Nakajima J, Matsuzawa T (2010) Anomalous deepening of a seismic

belt in the upper-plane of the double seismic zone in the Pacific slab beneath the Hokkaido corner: Possible evidence for thermal shielding caused by subducted forearc crust materials. Earth Planetary Sci Lett 290:415-426

Kubota T, Saito T, Suzuki W (2020) Millimeter-scale tsunami detected by a wide and dense observation array in the deep ocean: Fault modeling of an M_W 6.0 interplate earthquake off Sanriku, NE Japan. Geophys Res Lett: e2019GL085842

Kwiatek G, Plenkers K, Dresen G, JAGUARS Research Group (2011) Source Parameters of Picoseismicity Recorded at Mponeng Deep Gold Mine, South Africa: Implications for Scaling Relations. Bull Seismol Soc Am 101:2592-2608, doi.org/10.1785/0120110094

Madariaga R (1976) Dynamics of an expanding circular fault. Bull Seismol Soc Am 66:639-666

Mai, PM, Schorlemmer D, Page M, Ampuero JP, Asano K, Causse M, Custodio S, Fan W, Festa G, Galis M, Callovic F, Imperatori, W, Käser M, Malytskyy D, Okuwaki R, Pollitz F, Passone L Razafindrakoto HNT, Sekiguchi H, Song SG, Somala SN, Thingbaijam KKS, Twardzik C, van Driel M, Vyas JC, Wang R, Yagi Y, Zielk O (2016) The earthquake-source inversion validation (SIV) project. Seismol Res Lett 87:690-708.

Malagnini L, Scognamiglio L, Mercuri A, Akinci A, Mayeda K (2008) Strong evidence for non-similar earthquake source scaling in central Italy. Geophys Res Lett 35, doi:10.1029/2008GL034310

Matsubara M, Obara K (2011) The 2011 off the Pacific coast of Tohoku Earthquake related to a strong velocity gradient with the Pacific plate. Earth Planets Space 63:28, doi:10.5047/eps.2011.05.018

Moyer PA, Boettcher MS, McGuire, JJ, Collins, JA (2018) Spatial and temporal variations in earthquake stress drop on Gofar transform fault, East Pacific Rise: Implications for fault strength. J Geophys Res 123:7722-7740, doi:10.1029/2018JB015942

Nagai R, Kikuchi M, Yamanaka Y (2001) Comparative study on the source processes of recurrent large earthquakes in Sanriku-oki region: the 1968 Tokachi-oki earthquake and the 1994 Sanriku-oki earthquake. Zisin ser.2 54:267–280 (in Japanese with English abstract)

Nakajima J, Hasegawa A (2006) Anomalous low-velocity zone and linear alignment of seismicity along it in the subducted Pacific slab beneath Kanto, Japan: Reactivation of subducted fracture zone? Geophys Res Lett 33:16, doi.org/10.1029/2006GL026773

Nakajima J, Hirose F, Hasegawa A (2009) Seismotectonics beneath the Tokyo metropolitan area, Japan: Effect of slab-slab contact and overlap on seismicity. J Geophys Res 114, B8,

412 doi:10.1029/2008JB006101
413 Nishikawa T, Matsuzawa T, Ohta K, Uchida N, Nishimura T, Ide S (2019) The slow earthquake
414 spectrum in the Japan Trench illuminated by the S-net seafloor observatories. Science 365:808-813
415 Ohnaka M, Shen L (1999) Scaling of the shear rupture process from nucleation to dynamic propagation:
416 Implications of geometric irregularity of the rupturing surfaces. J Geophys Res 104, B1:817-844
417 Okuda T, Ide S (2018) Hierarchical rupture growth evidenced by the initial seismic waveforms. Nature
418 Comm, 9:1-7, doi:10.1038/s41467-018-06168-3
419 Oth A (2013) On the characteristics of earthquake stress release variations in Japan. Earth and
420 Planetary Sci Lett 377:132-141, doi:10.1016/j.epsl.2013.06.037
421 Prieto GA, Shearer PM, Vernon FL, Kilb, D (2004) Earthquake source scaling and self-similarity
422 estimation from stacking P and S spectra. J Geophys Res 109:B08310, doi:10.1029/2004JB003084
423 Shearer PM, Prieto, GA, Hauksson, E (2006) Comprehensive analysis of earthquake source spectra in
424 southern California. J Geophys Res 111, B06303. doi:10.1029/2005JB003979
425 Uchida N, Matsuzawa T, Ellsworth WL, Imanishi K, Okada T, Hasegawa A (2007) Source parameters
426 of a M4.8 and its accompanying repeating earthquakes off Kamaishi, NE Japan: Implications for the
427 hierarchical structure of asperities and earthquake cycle. Geophys Res Lett 34:20,
428 doi:10.1029/2007GL031263
429 Uchide T, Imanishi K (2018) Underestimation of microearthquake size by the magnitude scale of the
430 Japan Meteorological Agency: Influence on earthquake statistics. J Geophys Res 123:606-620,
431 doi:10.1002/2017JB014697
432 Uchide T, Shearer PM, Imanishi K (2014) Stress drop variations among small earthquakes before the
433 2011 Tohoku-oki, Japan, earthquake and implications for the main shock. J Geophys Res
434 119:7164-7174, doi:10.1002/2014JB010943
435 Urano S, Hiramatsu Y, Yamada T, The Group for the Joint Aftershocks Observations of the 2007 Noto
436 Hanto Earthquake (2015) Relationship between coseismic slip and static stress drop of similar
437 aftershocks of the 2007 Noto Hanto earthquake. Earth Planets Space 67:101.
438 doi:10.1186/s40623-015-0277-0
439 Wald DJ, Heaton TH (1994) Spatial and temporal distribution of slip for the 1992 Landers, California,
440 earthquake. Bull Seismol Soc Am 84:668-691
441 Walker KT, Shearer PM (2009) Illuminating the near-sonic rupture velocities of the intracontinental

Kokoxili M_W7.8 and Denali fault M_W7.9 strike-slip earthquakes with global P wave back projection imaging. J Geophys Res 114, B02304, doi:10.1029/2008JB005738

Wessel P, Smith W (1995) New version of the generic mapping tools. EOS Trans AGU 72:445–446

Yamada T, Mori JJ, Ide S, Abercrombie RE, Kawakata H, Nakatani M, Iio Y, Ogasawara H (2007) Stress drops and radiated seismic energies of microearthquakes in a South African gold mine. J Geophys Res 112:B03305, doi:10.1029/2006JB004553

Yamada T, Mori JJ, Ide S, Kawakata H, Iio Y, Ogasawara H (2005) Radiation efficiency and apparent stress of small earthquakes in a South African gold mine. J Geophys Res 110:B01305, doi:10.1029/2004JB003221

Yamada T, Okubo PG, Wolfe CJ (2010) Kīholo Bay, Hawai'i, earthquake sequence of 2006: Relationship of the main shock slip with locations and source parameters of aftershocks. J Geophys Res 115:B08304, doi:10.1029/2009JB006657

Yamada T, Yukutake Y, Terakawa T, Arai R (2015) Migration of earthquakes with a small stress drop in the Tanzawa Mountains, Japan. Earth Planets Space 67:175. doi:10.1186/s40623-015-0344-6

Yamada T, Saito Y, Tanioka Y, Kawahara J (2017) Spatial pattern in stress drops of moderate-sized earthquakes on the Pacific Plate off the south-east of Hokkaido, Japan: implications for the heterogeneity of frictional properties. Prog Earth Planet Sci 4:38, doi:10.1186/s40645-17-0152-7

Yamanaka Y, Kikuchi M (2004) Asperity map along the subduction zone in northeastern Japan inferred from regional seismic data. J Geophys Res 109:B7307, doi.org/10.1029/2003JB002683

Yoshimitsu N, Kawakata H, Takahashi N (2014) Magnitude -7 level earthquakes: A new lower limit of self-similarity in seismic scaling relationships. Geophys Res Lett 41:4495-4502, doi:10.1002/2014GL060306

Figure 1. (a) Seismicity around the study region from 2003 to 2018. Hypocenters with M equal to or greater than 3.0, as determined by JMA, are plotted. The size and color of the symbols show the magnitude and depth of earthquakes, respectively. It is clearly described that most earthquakes take place on the subduction interface of the Pacific Plate. (b) Epicenters of analyzed earthquakes and locations of seismic stations used in this study. The red circles show hypocenters, and the blue squares represent seismic stations, including stations of Hi-net (NIED), JMA, Hokkaido University, Hirosaki University, and Tohoku University. The depth of the upper surface of the subducting Pacific Plate is indicated by orange lines with an interval of 20 km Kita et al. (2010); Nakajima and Hasegawa (2006); Nakajima et al. (2009). Waveforms observed at the stations N.TROH and N.IWEH are displayed in Figs. 2, A1, A2, and A3.

Figure 2. (a) Example of an analyzed waveform of an earthquake with M4.8. The horizontal color bars show three time windows used in obtaining spectra, which were (S0) -0.50 to 9.73 s, (S1) 0.78 to 11.01 s, and (S2) 2.06 to 12.29 s after the arrival time of S wave. The gray line indicates a time window from 12.00 to 1.77 s before the P arrival, which was used to calculate the noise spectrum in (b). Individual time windows include 1,024 data points. (b) Waveform spectra for the four time windows marked in (a). (c) Example of a waveform of an M3.5 earthquake that was used for an EGF. Note that the vertical scale is different from that in (a). (d) Waveform spectra for the four time windows marked in (c). (e) Deconvolved spectra with the best-fit omega-squared model. The color lines show deconvolved source spectra, that is, (b) divided by (d), for three individual time windows with a resampling of frequency bands. The black broken line indicates the best-fit omega-squared model with corner frequencies of 1.0 and 2.5 Hz for the analyzed and EGF earthquakes, respectively.

Figure 3. (a) Stress drops for individual earthquakes estimated from P waves. The color and scale of circles express values of stress drop and earthquake magnitudes, respectively. The thick lines show the depth of the upper surface of the subducting Pacific Plate Kita et al. (2010); Nakajima and Hasegawa (2006); Nakajima et al. (2009). Thin contours indicate the coseismic displacement of the 2011 Tohoku earthquake with M_W9.0 Iinuma et al. (2012) at an interval of 2 m. (b) Spatially smoothed pattern of stress drop, which was derived from (a) at grid points at intervals of 0.1 degrees in latitude and longitude. Value at individual grid points were calculated as the average of stress drops of earthquakes within 20 km of the epicentral distance from the grid points. No values were assigned at grid points with less than four earthquakes within 20 km of the epicentral distance. (c) Values of stress drop obtained from S waves. (d) Spatially smoothed pattern of stress drop derived from (c).

Figure 4. Spatially smoothed stress drop derived from (a) P-wave and (b) S-wave analyses, the same as Figure 3. Thin contours show coseismic displacements of the following M7-8 large earthquakes for the 1968 Tokachi-oki, the 1978 Miyagi-oki, the 1981 Miyagi-oki, the 1989 Sanriku-oki, and the 2003 Miyagi-oki at an interval of 0.5 m Nagai et al. (2001); Yamanaka and Kikuchi (2004). Areas A and B, corresponding to areas where repeating earthquakes have been observed Uchida et al. (2007); Okuda and Ide (2018), have higher values of stress drop. Refer to the text in detail.

Figure 5. (a) Spatial distribution of smoothed stress drop estimated by S-wave analyses from 2003 to 2010, which is before the 2011 Tohoku earthquake. Thin contours show the coseismic displacement of the 2011 Tohoku earthquake at an interval of 2 m, the same as Figure 3 Iinuma et al. (2012). Please note that values were not assigned at grid points with less than four earthquakes within 20 km of the epicentral distance. (b) Stress drops from 2012 to 2018. Clear temporal changes are observed associated with the 2011 Tohoku earthquake in areas C and D, corresponding to edges of the coseismic slip. (c) Stress drops for all the analyzed period of 2003 through 2018.

Figure 6. (a) Values of stress drop estimated from S waves as a function of focal depth. The red circles show average values for each depth band for every 10 km. Vertical bars express standard errors for individual earthquakes, as obtained from results at individual seismic stations and components. (b) Values of stress drop estimated from S waves as a function of magnitude. The red circles indicate average values for individual magnitude ranges. Vertical bars show standard errors (same as (a)). (c) Stress drops as a function of time for all the analyzed earthquakes. (d) Temporal characteristics of stress drop in the area C. (e) Temporal features of stress drop in the area D.

Figure 7. Relationship between the JMA magnitude and the apparent magnitude derived as the sum of the magnitude of EGF earthquakes (3.5) and values of $(2/3)\log\left(R_r^C M_{0r}\right)$ in Equation (9). Results in (a) and (b) show those derived from P and S waves, respectively.

Figure A1. (a) Example of an analyzed waveform of an earthquake with M4.8, which was recorded by the UD component at the station N.TROH. The color lines indicate the three time windows used in deconvolution, which were (P0) -0.50 to 9.73 s, (P1) 0.78 to 11.01 s, and (P2) 2.06 to 12.29 s after the P arrival similar to Fig. 2. The gray line shows a time window from 12.00 to 1.77 s before the arrival time of the P wave, which was used to calculate the spectrum of a noise in (b). Each time window has 1,024 data points. (b) Spectra of waveforms for the four time windows shown in (a). (c) Example of a waveform of an M3.5 earthquake that was used for an EGF. Note that the vertical scales in (a) and (c) are different. (d) Spectra of waveforms for the four time windows shown in (c). (e) Deconvolved spectra with the fitted omega-squared model. The color lines are deconvolved source spectra, that is, (b) divided by (d), for three individual time windows with a resampling of frequency bands. The black broken line shows the fitted omega-squared model with corner frequencies of 1.0 and 3.2 Hz for the analyzed and EGF earthquakes, respectively.

Figure A2. (a) Example of an analyzed waveform of an earthquake with M4.4, which was recorded by the UD component at the station N.IWEH. (b) Spectra of waveforms for the four time windows shown in (a). (c) Example of a waveform of an M3.5 earthquake that was used for an EGF. Note that the vertical scales in (a) and (c) are different. (d) Spectra of waveforms for the four time windows shown in (c). (e) Deconvolved spectra with the fitted omega-squared model. The color lines are deconvolved source spectra, that is, (b) divided by (d), for three individual time windows with a resampling of frequency bands. The black broken line shows the fitted omega-squared model with corner frequencies of 10.0 and 15.8 Hz for the analyzed and EGF earthquakes, respectively.

Figure A3. (a) Example of an analyzed waveform of an earthquake with M4.4, which was recorded by the NS component at the station N.IWEH. (b) Spectra of waveforms for the four time windows shown in (a). (c) Example of a waveform of an M3.5 earthquake that was used for an EGF. Note that the vertical scales in (a) and (c) are different. (d) Spectra of waveforms for the four time windows shown in (c). (e) Deconvolved spectra with the fitted omega-squared model. The color lines are deconvolved source spectra, that is, (b) divided by (d), for three individual time windows with a resampling of frequency bands. The black broken line shows the fitted omega-squared model with corner frequencies of 6.3 and 12.6 Hz for the analyzed and EGF earthquakes, respectively.

Figures

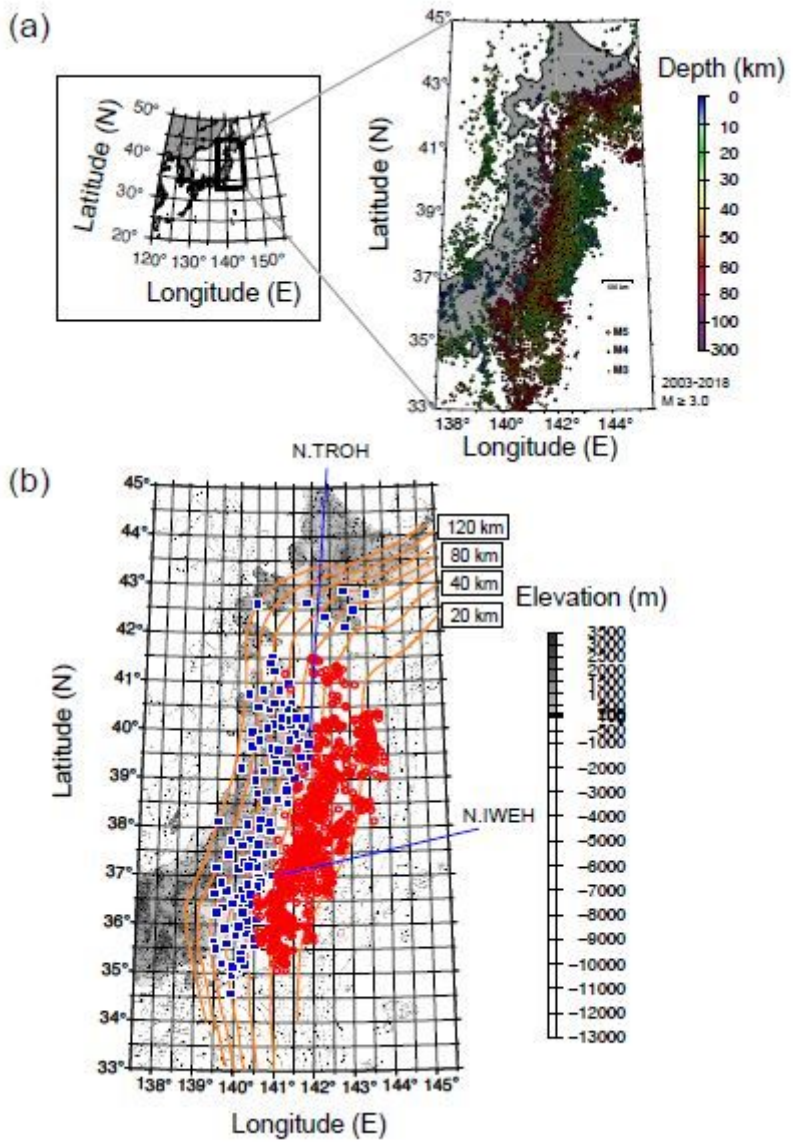

Figure 1

(a) Seismicity around the study region from 2003 to 2018. Hypocenters with M equal to or greater than 3.0, as determined by JMA, are plotted. The size and color of the symbols show the magnitude and depth of earthquakes, respectively. It is clearly described that most earthquakes take place on the subduction interface of the Pacic Plate. (b) Epicenters of analyzed earthquakes and locations of seismic stations used in this study. The red circles show hypocenters, and the blue squares represent seismic stations, including stations of Hi-net (NIED), JMA, Hokkaido University, Hirosaki University, and Tohoku University. The depth of the upper surface of the subducting Pacic Plate is indicated by orange lines with an interval of 20 km Kita et al. (2010); Nakajima and Hasegawa (2006); Nakajima et al. (2009). Waveforms observed at the stations N.TROH and N.IWEH are displayed in Figs. 2, A1, A2, and A3.

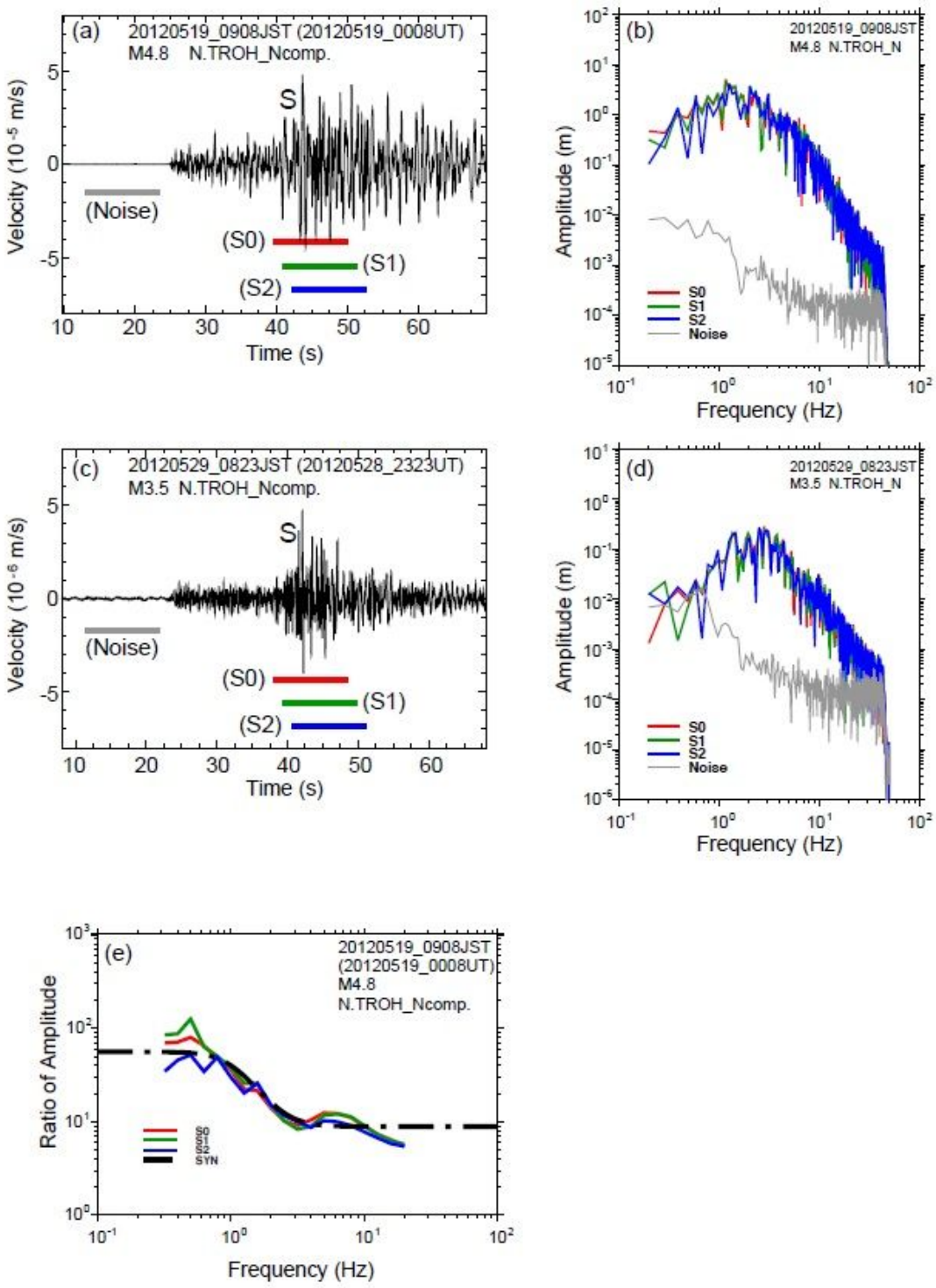

Figure 2

(a) Example of an analyzed waveform of an earthquake with M4.8. The horizontal color bars show three time windows used in obtaining spectra, which were (S0) -0.50 to 9.73 s, (S1) 0.78 to 11.01 s, and (S2) 2.06 to 12.29 s after the arrival time of S wave. The gray line indicates a time window from 12.00 to 1.77 s before the P arrival, which was used to calculate the noise spectrum in (b). Individual time windows include 1,024 data points. (b) Waveform spectra for the four time windows marked in (a). (c) Example of

a waveform of an M3.5 earthquake that was used for an EGF. Note that the vertical scale is di erent from that in (a). (d) Waveform spectra for the four time windows marked in (c). (e) Deconvolved spectra with the best-t omega-squared model. The color lines show deconvolved source spectra, that is, (b) divided by (d), for three individual time windows with a resampling of frequency bands. The black broken line indicates the best-t omega-squared model with corner frequencies of 1.0 and 2.5 Hz for the analyzed and EGF earthquakes, respectively.

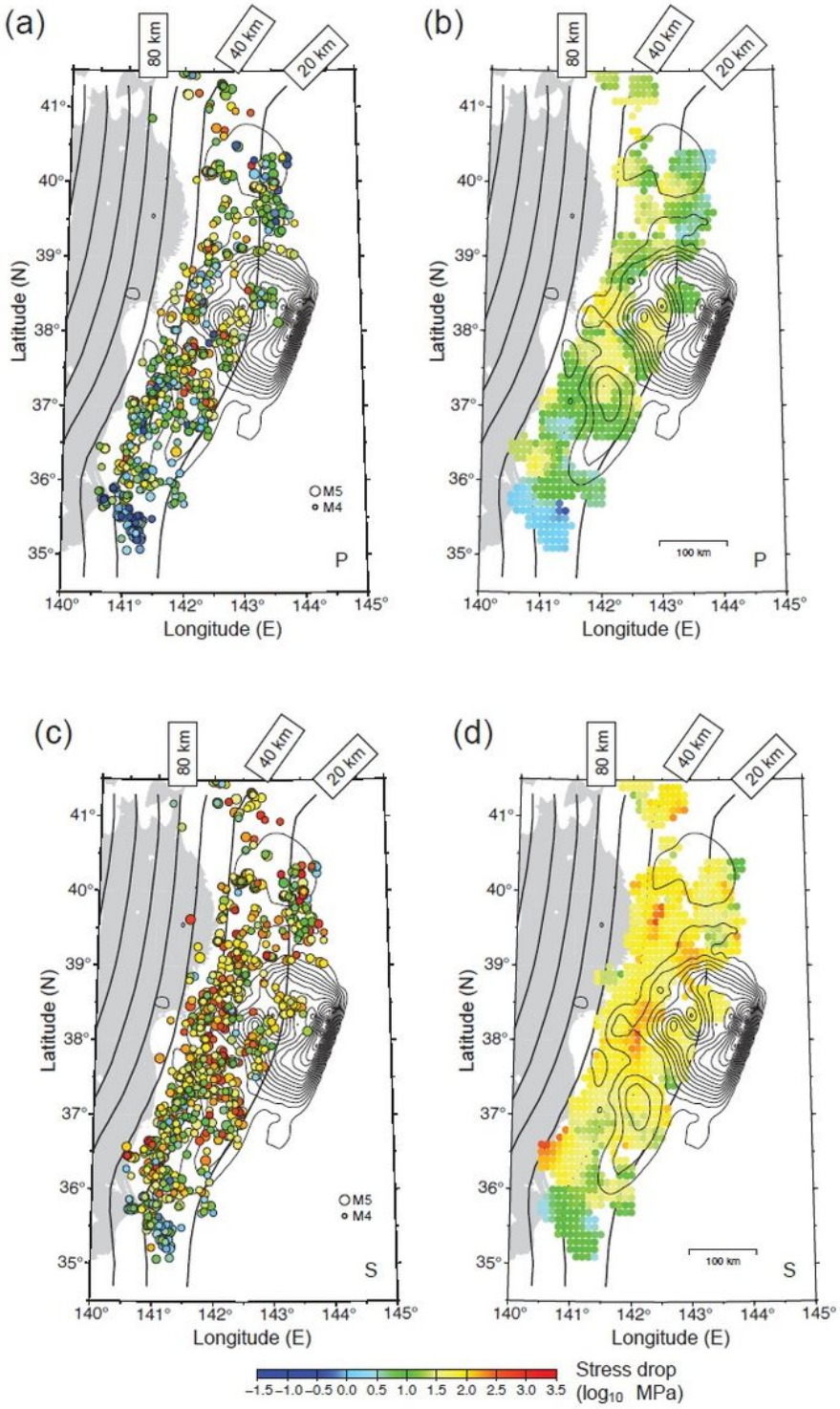

Figure 3

(a) Stress drops for individual earthquakes estimated from P waves. The color and scale of circles express values of stress drop and earthquake magnitudes, respectively. The thick lines show the depth of the upper surface of the subducting Pacic Plate Kita et al. (2010); Nakajima and Hasegawa (2006); Nakajima et al. (2009). Thin contours indicate the coseismic displacement of the 2011 Tohoku earthquake with MW9.0 Iinuma et al. (2012) at an interval of 2 m. (b) Spatially smoothed pattern of stress drop, which was derived from (a) at grid points at intervals of 0.1 degrees in latitude and longitude. Value at individual grid points were calculated as the average of stress drops of earthquakes within 20 km of the epicentral distance from the grid points. No values were assigned at grid points with less than four earthquakes within 20 km of the epicentral distance. (c) Values of stress drop obtained from S waves. (d) Spatially smoothed pattern of stress drop derived from (c).

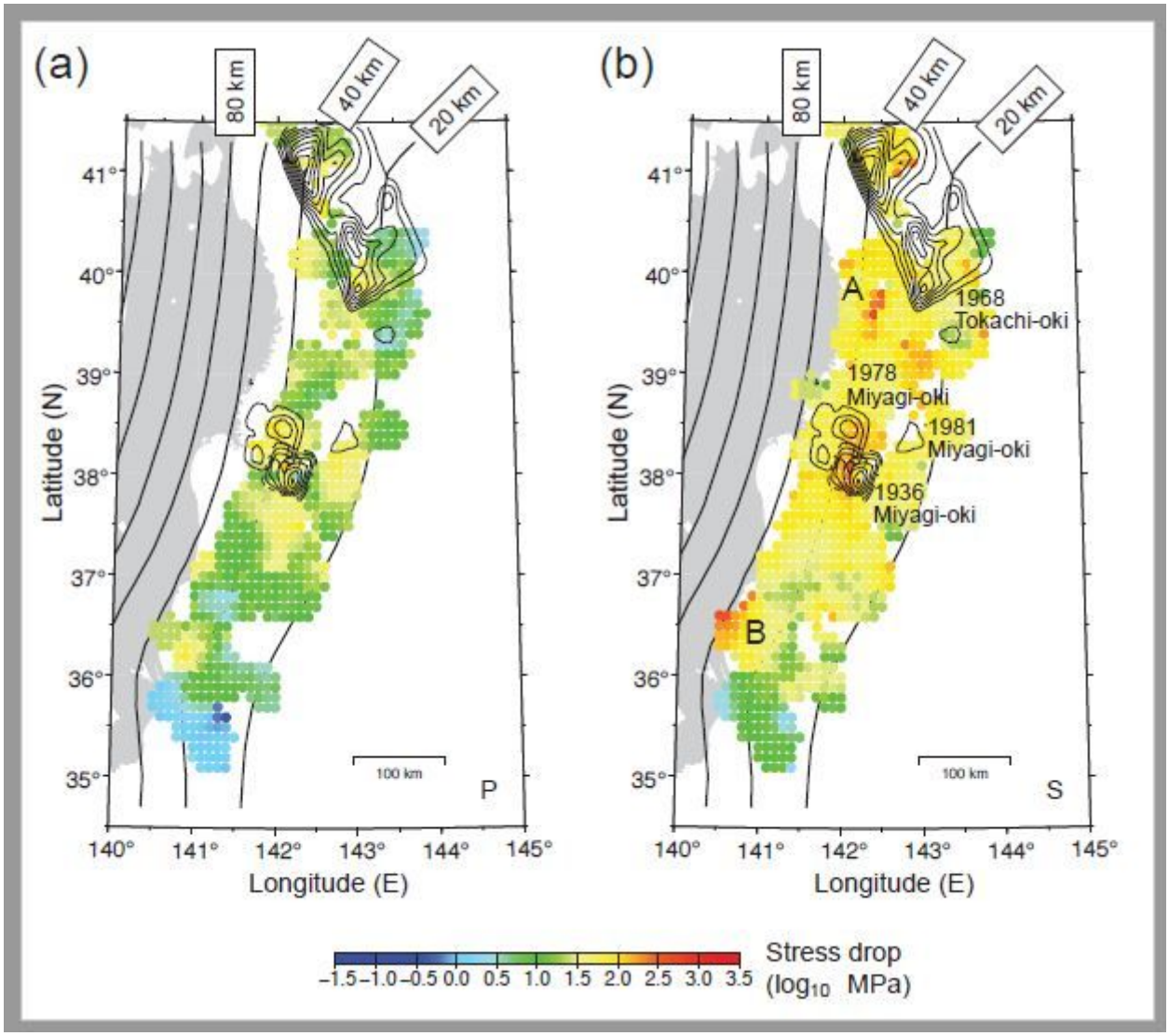

Figure 4

Spatially smoothed stress drop derived from (a) P-wave and (b) S-wave analyses, the same as Figure 3. Thin contours show coseismic displacements of the following M7-8 large earthquakes for the 1968 Tokachi-oki, the 1978 Miyagi-oki, the 1981 Miyagi-oki, the 1989 Sanriku-oki, and the 2003 Miyagi-oki at an interval of 0.5 m Nagai et al. (2001); Yamanaka and Kikuchi (2004). Areas A and B, corresponding to

areas where repeating earthquakes have been observed Uchida et al. (2007); Okuda and Ide (2018), have higher values of stress drop. Refer to the text in detail.

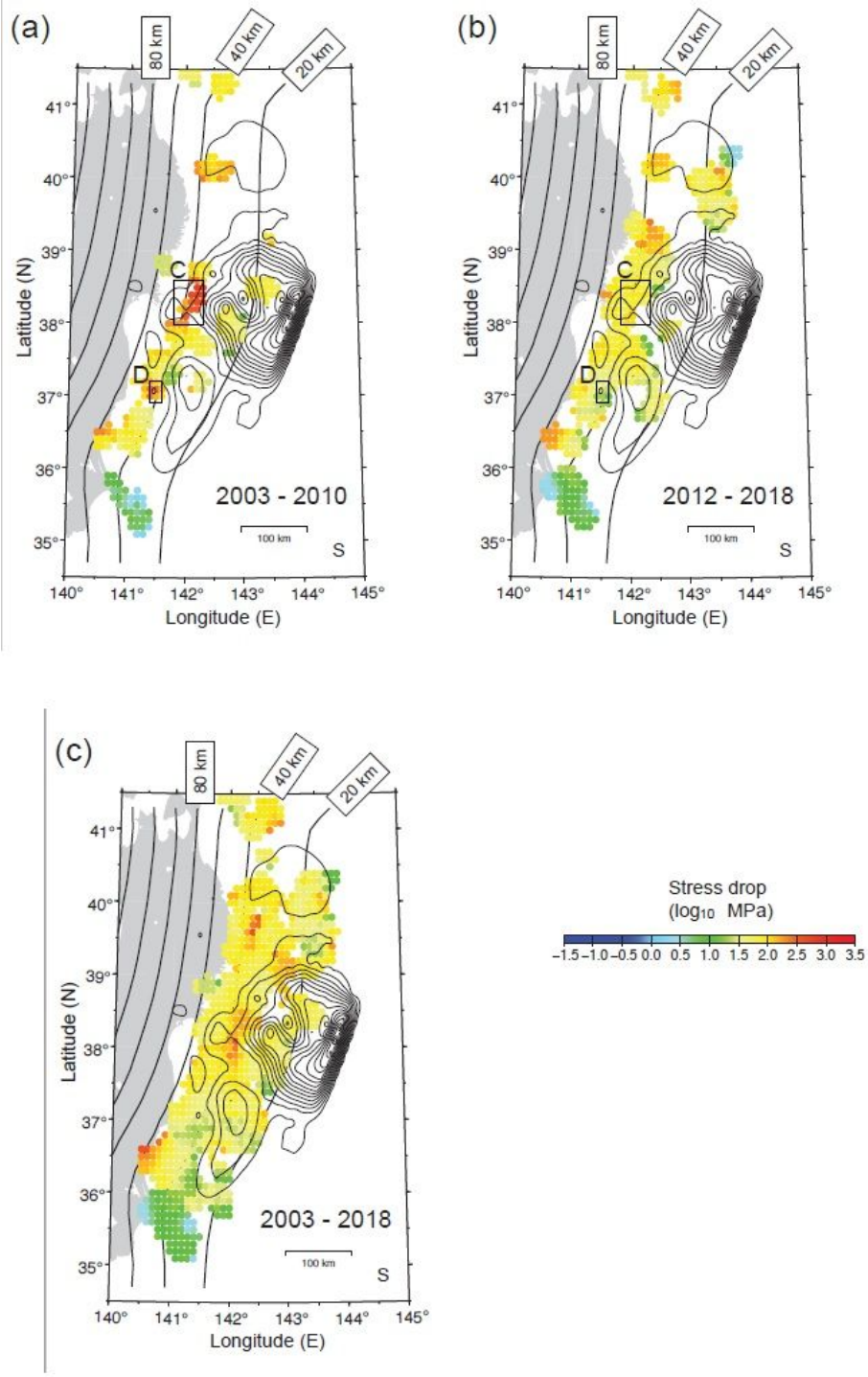

Figure 5

(a) Spatial distribution of smoothed stress drop estimated by S-wave analyses from 2003 to 2010, which is before the 2011 Tohoku earthquake. Thin contours show the coseismic displacement of the 2011 Tohoku earthquake at an interval of 2 m, the same as Figure 3 Iinuma et al. (2012). Please note that

values were not assigned at grid points with less than four earthquakes within 20 km of the epicentral distance. (b) Stress drops from 2012 to 2018. Clear temporal changes are observed associated with the 2011 Tohoku earthquake in areas C and D, corresponding to edges of the coseismic slip. (c) Stress drops for all the analyzed period of 2003 through 2018.

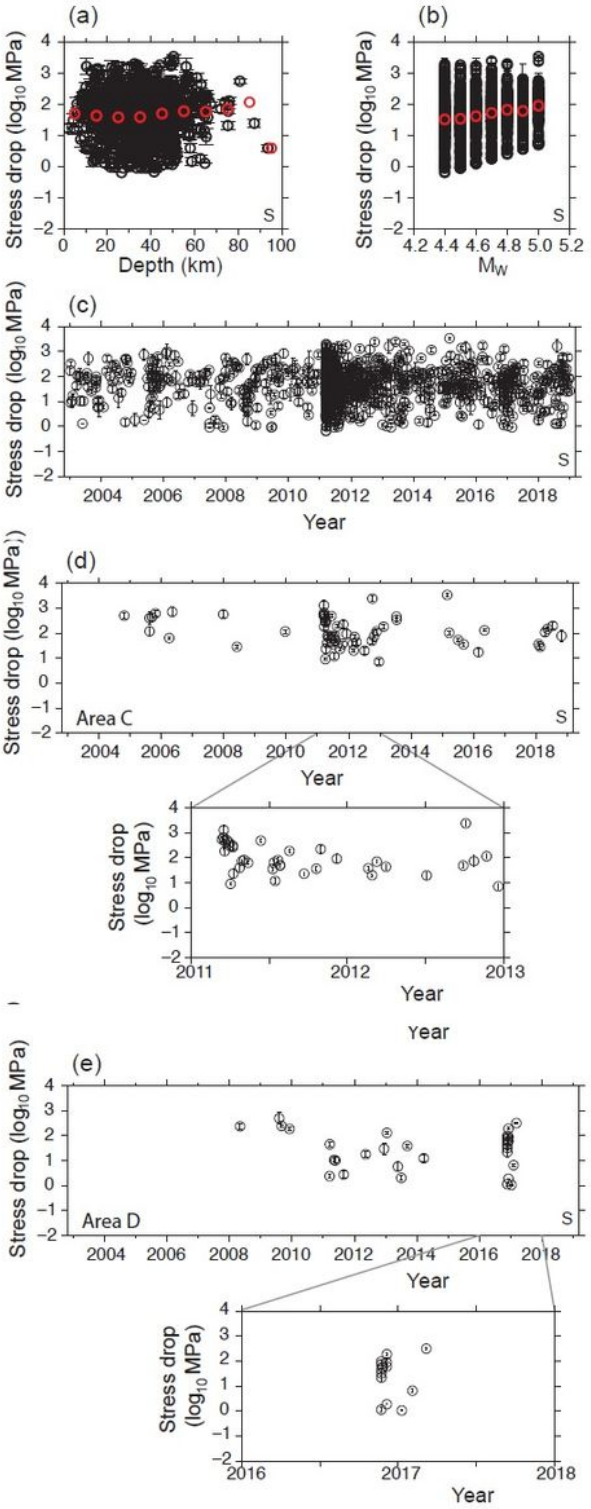

Figure 6

(a) Values of stress drop estimated from S waves as a function of focal depth. The red circles show average values for each depth band for every 10 km. Vertical bars express standard errors for individual earthquakes, as obtained from results at individual seismic stations and components. (b) Values of stress drop estimated from S waves as a function of magnitude. The red circles indicate average values for individual magnitude ranges. Vertical bars show standard errors (same as (a)). (c) Stress drops as a function of time for all the analyzed earthquakes. (d) Temporal characteristics of stress drop in the area C. (e) Temporal features of stress drop in the area D.

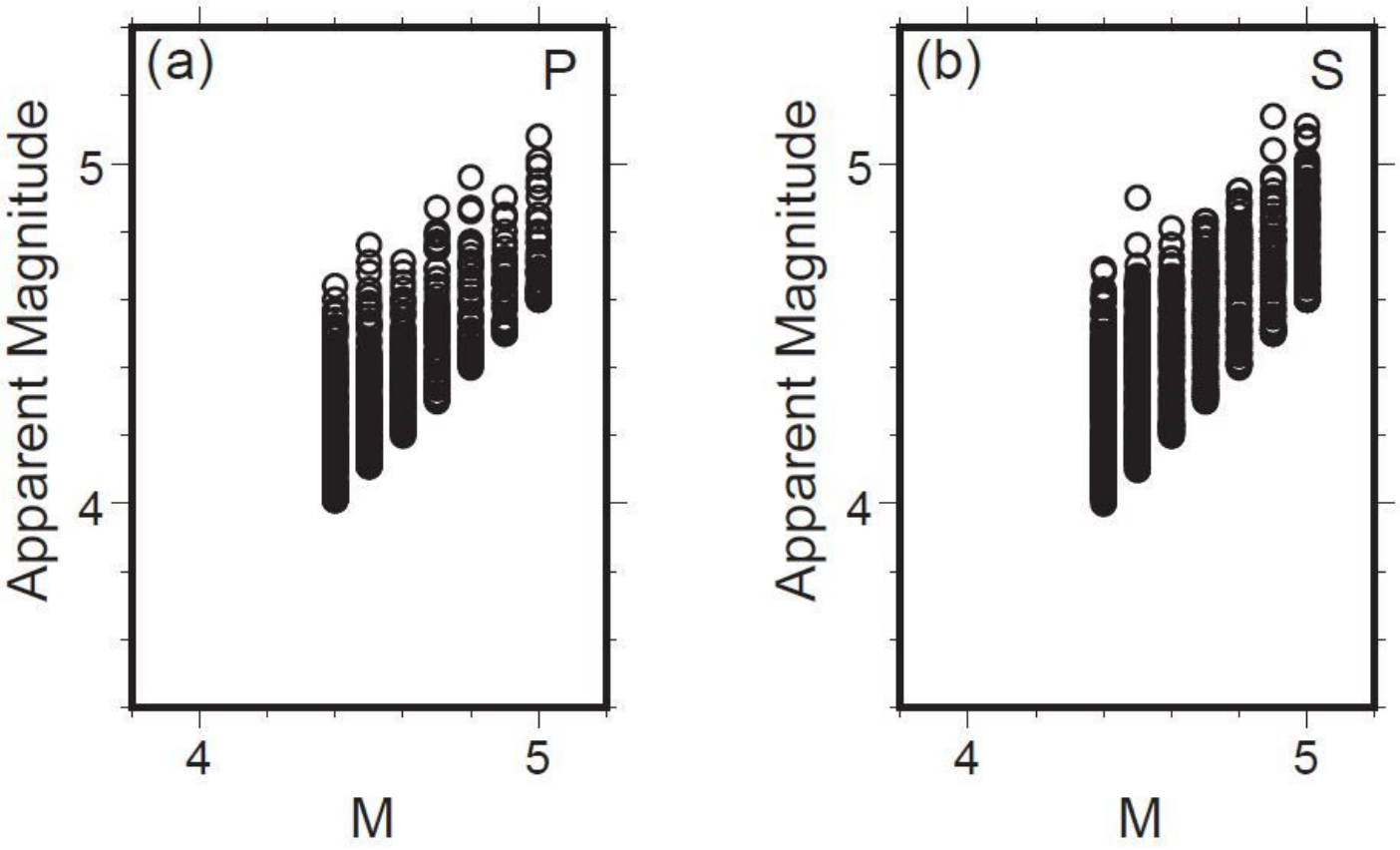

Figure 7

Relationship between the JMA magnitude and the apparent magnitude derived as the sum of the magnitude of EGF earthquakes (3.5) and values of (2=3) log RCr M0r in Equation (9). Results in (a) and (b) show those derived from P and S waves, respectively.

Supplementary Files

This is a list of supplementary files associated with this preprint. Click to download.

- 13eqlist.txt
- 15resultsS.txt
- 14resultsP.txt
- 12figSupp03deconvM44S.pdf

- 16graphycalabstract.pdf
- 11figSupp02deconvM44P.pdf
- 10figSupp01deconvM48P.pdf